NA/Chipley

24 AUG 1999

REPORT DOCUMENTATION PAGE

AFRL-SR-BL-TR-99-

0324

1. REPORT DATE *(DD-MM-YYYY)*
30-06-1999

2. REPORT DATE
6/30/99

3. DATES COVERED (From - To)
Nov. 1 97 - Nov. 31 98

4. TITLE AND SUBTITLE
Dynamic Strength Enhancement of Conventional Concrete

5a. CONTRACT NUMBER

5b. GRANT NUMBER
F49620-98-1-0159

5c. PROGRAM ELEMENT NUMBER

5d. PROJECT NUMBER

5e. TASK NUMBER

5f. WORK UNIT NUMBER

6. AUTHOR(S)
H.D. Kang, Y.S. Roh, K.J. Willam and Y. Xi

7. PERFORMING ORGANIZATION NAME(S) AND ADDRESS(ES)
CEAE Department
CU-Boulder
Boulder, CO 80309-0428

8. PERFORMING ORGANIZATION REPORT NUMBER
SESM Research Series
Report CU/SR-99/6

9. SPONSORING/MONITORING AGENCY NAME(S) AND ADDRESS(ES)
US AFOSR
Bolling Air Force Base
Washington, DC 20332-6448

10. SPONSOR/MONITOR'S ACRONYM(S)

11. SPONSORING/MONITORING AGENCY REPORT NUMBER

12. DISTRIBUTION AVAILABILITY STATEMENT
Unrestricted

19990927 047

13. SUPPLEMENTARY NOTES

14. ABSTRACT
In order to investigate the performance of conventional concrete at different loading rates, experimental results of strength enhancement were obtained under tension and compression tested under different loading speeds. G-mix specimens prepared at the Tyndall Air Force Base were used to determine the range of loading rates of the servo-hydraulic equipment at hand and to obtain experimental results with a series of indirect tension and uniaxial compression tests.

For interpretation of the experimental observations, a comprehensive triaxial concrete model was extended from rate independent elasto-plasticity to rate dependent visco-plasticity using the Duvaut-Lions overstress formulation. The visco-plastic concrete model was adopted to explore the dynamic strength enhancement in tension, compression and shear in terms of a single viscosity or rather relaxation time. In concrete the failure properties, i.e. the triaxial strength and the failure mode, depend not only on the load path, but also on the loading rate especially at high speed impact. In this paper an effort was undertaken to assess the diffuse and localized failure modes of the triaxial concrete model and its visco-plastic extension.

15. SUBJECT TERMS
Rate Effects of Concrete Materials, Viscoplastic Concrete Model, Dynamic Strength Enhancement in Tension, Compression and Shear

16. SECURITY CLASSIFICATION OF:			17. LIMITATION OF ABSTRACT	18. NUMBER OF PAGES	19a. NAME OF RESPONSIBLE PERSON
a. REPORT	b. ABSTRACT	c. THIS PAGE			19b. TELEPONE NUMBER *(Include area code)*

Standard Form 298 (Rev. 8-98)
Prescribed by ANSI-Std Z39-18

DTIC QUALITY INSPECTED 4

Dynamic Strength Enhancement of Conventional Concrete

Hong D. Kang [1], Young S. Roh[2], Kaspar J. Willam [3] and Yunping Xi[4]

Abstract

In order to investigate the performance of conventional concrete at different loading rates, experimental results of strength enhancement were obtained under tension and compression tested under different loading speeds. G-mix specimens prepared at the Tyndall Air Force Base were used to determine the range of loading rates of the servo-hydraulic equipment at hand and to obtain experimental results with a series of indirect tension and uniaxial compression tests.

For interpretation of the experimental observations, a comprehensive triaxial concrete model was extended from rate independent elasto-plasticity to rate dependent visco-plasticity using the Duvaut-Lions overstress formulation. The visco-plastic concrete model was adopted to explore the dynamic strength enhancement in tension, compression and shear in terms of a single viscosity or rather relaxation time. In concrete the failure properties, i.e. the triaxial strength and the failure mode, depend not only on the load path, but also on the loading rate especially at high speed impact. In this paper an effort was undertaken to assess the diffuse and localized failure modes of the triaxial concrete model and its visco-plastic extension.

Keywords: Duvaut Lions visco-plasticity, Concrete, Rate sensitivity, Dynamic strength enhancement, Regularization.

[1]Post-doctoral Fellow, CEAE Dept. University of Colorado, Boulder, CO 309-0428
[2]Doctoral Student, CEAE Dept. University of Colorado, Boulder, CO 309-0428
[3]Professor, CEAE Dept. University of Colorado, Boulder, CO 80309-0428
[4]Assistant Professor, CEAE Dept. University of Colorado, Boulder, CO 80309-0428

1 Introduction

Mechanical loading initiates micromechanical failure of concrete materials due to interface debonding among the cement paste and the aggregate particles. Thereby, the heterogeneous constituents of materials alter material rate effects due to different mass densities. The different failure mechanisms of particle interaction and the interface layers determine the surface roughness which may be used as a measure of fracture energy release during failure. As the fracture energy presumably remains constant when the surface area of fracture zone does not change, the strength enhancement under fast loading will be accompanied by increasing brittleness unless the fracture surface area changes.

The experimental exploration of the dynamic strength enhancement in concrete materials is limited to the loading range of the servo-hydraulic MTS testing systems in the Materials Laboratory of the University of Colorado at Boulder which is capable of loading up to strain rate of $\dot{\epsilon} = 10^{-1}$ at the fastest. Thus only a limited amount of strength enhancement is expected in the experimental test program. Thereby previously tested results collected by Bischoff (1988) and Bachmann (1993) are used to compare experimental and numerical results conducted for the project sponsored by AFOSR under grant F 49620-98-1-0159: 'Dynamic Performance of Conventional and Non-conventional Concrete'.

To compare predictions of rate independent with rate dependent concrete behaviors under different loading rates, the triaxial elasto-plastic concrete formulation by Kang (1997) is adopted which has been implemented in the 3-D FE program FEAP[5]. A single eight noded brick finite element is used to study the difference of viscous effects in uniaxial tension, shear and uniaxial compression assuming uniform conditions. For shear loading, equibiaxial tension-compression (T-C) is applied to evaluate the dynamic strength enhancement of concrete subject to in-plane shearing under plane stress. A literature survey shows that the increase of strength in concrete materials is not very significant for loading rates up to $\dot{\epsilon} = 1 \times 10^{-2}\,(mm/mm/sec)$. However, for loading rates higher than $\dot{\epsilon} = 1 \times 10^{-1}\,(mm/mm/sec)$, especially the dynamic strength enhancement of tensile strength becomes very significant.

2 Experiments

A series of tests under splitting tension and uniaxial compression were performed on G-mix specimens which were prepared at the Tyndall Air Force Base. Single-sized limestone aggregates were used, the diameter of which was smaller than 1 *cm* (3/8 *in.*). The aggregates were retained on a # 4 (3/16 in.) sieve. Concrete was mixed with more water than the amount of regular concrete mix ratio to minimize air void. It is type I Portland cement,

[5]Finite Element Analysis Program developed by R. Taylor and G. Simo, University of California, Berkeley

$C:S:G = 1:3.6:4.6$, $w/c = 1.0$ by weight, and 6.1 % of type 'F' flyash. Three different G-mix specimens were provided: (a) eight $15cm \times 30cm$ ($6in \times 12in$) cylinders, (b) twelve $10cm \times 10cm \times 20cm$ ($4in \times 4in \times 8in$) prisms, and (c) nine $10cm \times 10cm \times 10cm$ ($4in \times 4in \times 4in$) cubes.

Axial deformation was measured by two LVDTs (Linear Variable Differential transducer) attached on both sides of the specimen as depicted in Figure 1. For compression testing, some grease was applied to the loading surface (i.e. top & bottom) to minimize friction between loading platen and specimen. In the case of the indirect Brazilian tension test, the test method described in ASTM C496 (1996) was followed for the cylindrical specimen geometry. In contrast, for tension testing on cubical specimen, a circular loading device (diameter, D_o = 60 mm) depicted in Figure 1, was used according to RILEM recommendation TC14-CPC (1994). For both splitting tension and compression tests, stroke control was used by maintaining constant stroke with various loading rates. During the test, the response behavior of vertical load *vs.* stroke was monitored and recorded by the data acquisition system.

2.1 Compression Test

Four cylindrical and twelve prismatic specimens were used for uniaxial compression testing. The moderate strain rate was $\dot{\epsilon} = 1 \times 10^{-3}$ (mm/mm/sec) and the low strain rate was $\dot{\epsilon} = 1 \times 10^{-6}$. The first cylindrical specimen (GCR1) under uniaxial compression was tested with a wrong parameter setup of the data acquisition system, so the compressive strength, f'_c of that specimen underestimates the actual strength as shown in Table 1. In contrast, the compressive strength values obtained from the prismatic specimens were significantly higher than the ones of the cylindrical specimens, see Table 2. There was 40 % difference in strengths which can not be fully explained by shape and size of the two different geometries. As indicated in Figure 2, the dynamic strength enhancement of the cylindrical specimens shows about 15 % increase, while the strength values of the prismatic specimens exhibit slightly more enhancement. The stress-strain responses of the experiments are shown for various loading rates in Figures 3 (a and b).

2.2 Indirect Splitting Tension Test

Four cylindrical and nine cubical specimens were used for indirect Brazilian tension testing. Figure 4 exhibits the relative increase of tensile strength at different loading rates, and Figures 5 (a and b) illustrate the nominal stress *versus* axial strain (i.e. stroke over the specimen height, D_o) of cubical and cylindrical specimens, respectively. The tensile strength of G-mix concrete was evaluated by the standard formula in Eqn. (1) based on linear elasticity (Timoshenko and Goodier, 1970) considering the specific geometry of the cylindrical and cubical

specimens and the maximum applied load, see also Bažant and Kazemi (1990); Carmona et al. (1998). It was surprising that the cylindrical specimens did yield significantly higher tensile strength values of $f_t' = 3.79\ MPa$ (550 psi) at low loading rates than the cubical specimens at $f_t' = 2.41\ MPa$ (350 psi), although the "dynamic" strength values did vary considerably from specimen to specimen, see Tables 3 and 4. For relatively small size specimens this curious inverse size effect of the splitting tension test was also observed by Carmona et al. (1998) such that a larger size of specimen exhibits a larger value of strength. In contrast the traditional size effect results of decreasing strength with increasing size by Bažant and Planas (1998) for splitting tension tests did cover a much larger range of geometry scales. The converted splitting tensile strength is evaluated from

$$f'_{t,con} = \frac{2P}{\pi b D} \tag{1}$$

whereby the size width of the packing strip plays an important role. We should also note that the radius of the steel rods underneath the loading platen leads to higher stress concentration in the cubical specimens as compared to the cylindrical one.

3 Visco-Plasticity of Concrete

As rate effect of concrete material is one of the main ingredients in the field of dynamic impact and ballistic loadings, the material characterization needs to take care of the rate-sensitive behavior. Thereby visco-plasticity is a key feature to account for rate effect in cohesive-frictional materials. Among several rate formulations, the Perzyna-model (1966) is the most prominent extension of classical Bingham visco-plasticity, while the Duvaut-Lions formulation (Duvaut-Lions (1972); Etse and Willam (1999)) and the 'fully consistent' visco-plastic overstress formulation by Wang et al. (1997) have been recently proposed to improve the asymptotic behavior of visco-plastic formulations. Among these, the Duvaut-Lions linear overstress model is used in this study to model the results of loading rate experiments on concrete.

3.1 Concrete Model

The concrete failure criterion by Kang (1997) delimits the triaxial strength in stress space and describes the loading surface for isotropic hardening/softening in a smooth fashion. The curvilinear loading surface $F(\boldsymbol{\sigma}, \boldsymbol{q}) = 0$, which is C^1-continuous except at the apex in equi-triaxial tension, is calibrated with the aid of conventional triaxial compression tests by Willam et al. (1986). The triaxial concrete formulation includes pressure sensitivity, inelastic dilatancy, growth of deviatoric strength, brittle-ductile transition, limitation of hardening and strain softening in equi-triaxial compression. The smooth cap in high triaxial compression opens up

eventually when the hardening surface reaches the triaxial failure envelope which is fixed in stress space. On the tension side, the conical failure envelope collapses below the transition point of brittle-ductile failure in a smooth manner. The failure criterion is comprised of three components:

$$F(\xi,\rho,\theta) = F(\xi,\rho,\theta)_{\mathsf{fail}} + F(\xi,\rho,k(q_h))_{\mathsf{hardg}} + F(\xi,\rho,c(q_s))_{\mathsf{softg}} = 0 \tag{2}$$

The curvilinear shape of the failure envelope is a function of the three stress invariants $I_1 = tr\boldsymbol{\sigma}$, $J_2 = \frac{1}{2}\mathrm{s}:\mathrm{s}$, $J_3 = \det(\mathrm{s})$ that are here expressed in terms of the Haigh-Westergaard coordinates, $\xi = I_1/\sqrt{3}$, $\rho = \sqrt{2J_2}$, and $\theta = (1/3)cos^{-1}\{(3\sqrt{3}J_3)/(2J_2^{1.5})\}$. The failure envelope fixes the triaxial strength in stress space in terms of a curvilinear triple-symmetric cone which is depicted in Figure 6(a) in the form of the meridional section, and in Figure 6(b), in the form of deviatoric tracings at different levels of hydostatic stress. The overall performance of the concrete model is illustrated in Figure 7 in the form of tensile and compressive meridians. The failure envelope is described by power function

$$F(\xi,\rho,\theta)_{\mathsf{fail}} = \frac{\rho r(\theta,e)}{f'_c} - \frac{\rho_1}{f'_c}\left(\frac{\xi-\xi_o}{\xi_1-\xi_o}\right)^{\alpha} = 0 \tag{3}$$

with the exponent, $\alpha = 0.77$ which determines the shape of the curvilinear meridian somewhat flatter than a quadratic parabola (i.e. $\alpha = 0.5$). The order of the power function and thus the shape of the meridian was determined by fitting and refining the failure envelope to triaxial concrete test data by Launay and Gachon (1971). Details are described in Kang and Willam (1999).

The shape of the deviatoric trace is described by the radial distance from the hydrostat (Willam and Warnke 1975)

$$r(\theta,e) \;=\; \frac{4(1-e^2)cos^2\theta \;+\; (2e-1)^2}{2(1-e^2)\cos\theta + (2e-1)\sqrt{4(1-e^2)\cos^2\theta + 5e^2 - 4e}} \tag{4}$$

The dependence of the radial distance on the third invariant θ allows the deviatoric trace to expand from triangular to circular shapes with increasing hydrostatic compressive pressure as shown in Figure 6(b).

3.2 Visco-plastic Extension

Analogous to infinitesimal elasto-plasticity, the total strain rate is decomposed additively into an elastic and into a visco-plastic part,

$$\dot{\epsilon} = \dot{\epsilon}_e + \dot{\epsilon}_{vp} \tag{5}$$

Considering linear elasticity it follows that

$$\dot{\boldsymbol{\sigma}} = \boldsymbol{\mathcal{E}} : [\dot{\boldsymbol{\epsilon}} - \dot{\boldsymbol{\epsilon}}_{vp}] \tag{6}$$

In the Duvaut-Lions formulation the visco-plastic strain rate and the rate of state variables are defined in the form of the linear overstress model

$$\begin{aligned} \dot{\boldsymbol{\epsilon}}_{vp} &= \frac{1}{\tau}\boldsymbol{\mathcal{E}}^{-1} : [\boldsymbol{\sigma} - \bar{\boldsymbol{\sigma}}] \\ \dot{\boldsymbol{q}} &= \frac{1}{\tau}[\boldsymbol{q} - \bar{\boldsymbol{q}}] \end{aligned} \tag{7}$$

whereby τ designates the relaxation time, and $(\bar{\boldsymbol{\sigma}}, \bar{\boldsymbol{q}})$ stand for the 'backbone' stress and the set of internal state variables associated with the elasto-plastic problem. Thus, the differential stress-strain relationship in Eqn. (6) expands into the linear overstress format

$$\dot{\boldsymbol{\sigma}} = \boldsymbol{\mathcal{E}} : \dot{\boldsymbol{\epsilon}} - \frac{1}{\tau}[\boldsymbol{\sigma} - \bar{\boldsymbol{\sigma}}] \tag{8}$$

3.3 Incremental Format in Constitutive Driver

The backward Euler strategy of time integration transforms the differential equation in Eqn. (8) into algebraic form and advances the solution in the time step $\Delta t = t_{n+1} - t_n$:

$$\Delta\boldsymbol{\sigma}_{n+1} = \boldsymbol{\mathcal{E}} : \Delta\boldsymbol{\epsilon}_{n+1} - \frac{\Delta t}{\tau}[\boldsymbol{\sigma}_{n+1} - \bar{\boldsymbol{\sigma}}_{n+1}] \tag{9}$$

Tangential linearization for the iterative Newton-Raphson solution of the nonlinear Backward Euler equations leads to the algorithmic elastic-viscoplastic tangent operator of Duvaut-Lions,

$$\left[\boldsymbol{\mathcal{E}}_{vp}^{alg}\right]^{DL} = \frac{d\boldsymbol{\sigma}}{d\boldsymbol{\epsilon}} = \left[\frac{\tau}{\tau + \Delta t}\boldsymbol{\mathcal{E}} + \frac{\Delta t}{\tau + \Delta t}\boldsymbol{\mathcal{E}}_{ep}^{alg}\right] \tag{10}$$

where the subscript $t = t_{n+1}$ is omitted for the sake of clarity. Note, this expression involves the algorithmic elasto-plastic tangent operator $\boldsymbol{\mathcal{E}}_{ep}^{alg}$ which determines the backbone stress $\bar{\boldsymbol{\sigma}}_{n+1}$. Moreover, the limiting condition $\Delta t/\tau \to 0$ results in instantaneous elasticity $d\boldsymbol{\sigma} = \boldsymbol{\mathcal{E}} : d\boldsymbol{\epsilon}$, while $\Delta t/\tau \to \infty$ results in instantaneous elasto-plasticity $d\boldsymbol{\sigma} = \boldsymbol{\mathcal{E}}_{ep}^{alg} : d\boldsymbol{\epsilon}$.

In the Duvaut Lions formulation, Δt determines the loading rate, and the relaxation time, τ controls the visco-plastic process and settles the stress state at $t = t_{n+1}$. As depicted in

Figure 8, after reaching the trial stress state, σ_T, unlike the result of the elasto-plastic return process, the stress state remains somewhere between the trial and failure envelopes according to the values of Δt and τ. The visco-plastic constitutive process prevents the solutions from localizing right away since the stress path does not follow the elasto-plastic yield constraint, i.e. $F_{n+1} = 0$, while elasto-plasticity yields discontinuous bifurcation near the peak strength. When τ is very large, the stress state at $t = t_{n+1}$ may stay near the trial stress state, so the combination of Δt and τ determines the amount of viscosity which is needed for characterizing the loading *rate* or for *regularizing* the constitutive formulations.

4 Performance of Visco-plastic Concrete Model

As experimental results of indirect tension and uniaxial compression under different loading rates are limited to a certain range of strain rate due to the limited number of specimens and the limited capacity of the testing machine, other test results by Bischoff (1988) and Bachmann (1993) are used in this study in order to explore the rate sensitive behavior of the specific G-mix concrete. Thereby the numerical results of the Duvaut Lions concrete model are presented to predict the rate sensitive behavior of concrete, and to compare the results with experimental data. As indicated by the experimental data of Bischoff (1988) and Bachmann (1993) in Figures 2 and 4, the strength enhancements are very different in tension and compression at strain rate of $\dot{\epsilon} = 10^0 \ to \ 10^1$, while our in-house experimental results show only a moderate 15 to 20 % strength increase at $\dot{\epsilon} = 10^{-2}$.

4.1 Strength Enhancement

The results in Figures 9(a), 10(a), and 11(a) illustrate the dynamic strength enhancement when the Duvaut-Lions extension of the triaxial concrete model is subject to uniaxial tension, shear (T-C) and uniaxial compression at different loading rates. The tensile response in Figure 9(a) illustrates a modest strength enhancement with increasing strain rate $\dot{\epsilon} = 10^{-3}\, to\, 10^{-1}$. However at $\dot{\epsilon} = 10^0 \ to \ 10^1$ for $\tau = 10^{-1}\, to\, 10^{-4}\, sec$, it shows a drastic increase of 3-4 times the static tensile strength. The stress *vs.* strain response curves in Figure 9(b) demonstrate increasing strength and localization which appears at two slow loading rates as indicated by the symbol $\ominus$. Thus the localization points at the end of softening in visco-plasticity, Figures 9 (e and f), exhibit negative eigenvalues of the localization tensor, $\boldsymbol{Q}_{vp} = \boldsymbol{N} \cdot \boldsymbol{\mathcal{E}}_{vp}^{alg} \cdot \boldsymbol{N}$. Thereby the localization diagrams in Figures 9 (e and f) plot the variation of the normalized algorithmic localization indicator $\det(\boldsymbol{Q}_{vp}^{alg})/\det(\boldsymbol{Q}_e)$ of the Duvaut-Lions formulation of the concrete model as a function of the angle of inclination θ between the normal to the discontinuity surface with the axis of minor stress. Up to the localization point, the Duvaut-Lions visco-plastic extension of concrete material prevents loss of ellipticity of the underlying differential equations. The

shear (T-C) result in Figure 10(a) illustrates a similar increase of shear strength as the tension test, however at a lower rate of loading, $\dot{\epsilon} = 10^{-3}$ *to* 10^{-2} for $\tau = 10^0 sec$. Finally the results of uniaxial compression in Figures 11 (a and b) exhibit only a very modest increase of 8 % in compressive strength at $\dot{\epsilon} = 10^{-1}$ *to* 10^1 for $\tau = 10^{-1} sec$. Unlike tension and shear(T-C), very fast loading in uniaxial compression causes numerical convergence problems due to the high degree of nonlinearity enforcing lateral dilatation. Obviously the localization properties of uniaxial compression remain positive, i.e. indicating no loss of ellipticity, as this loading case does not trigger localization even in the rate-independent elasto-plastic case as shown in Figure 11(c).

The strain rate at which the strength enhancement starts is controlled by Δt and τ in the numerical simulation. However due to the highly nonlinear behavior of concrete materials, the small number of loading steps to complete the entire response behavior causes numerical instabilities during hardening and softening. Figure 11(a) indicates that the compressive strength starts increasing at $\dot{\epsilon} = 10^{-1}$, however results are only available up to $\dot{\epsilon} = 10^0$ due to the numerical difficulties in obtaining the compressive response at high loading rate. As indirect tension generates the inelastic redistribution due to dilatancy and thus less material nonlinearities than uniaxial compression, results could be obtained at higher loading rates.

4.2 Regularization

The visco-plastic extension of the inviscid elasto-plastic model regularizes the localized solutions by preventing the underlying differential equations from loss of ellipticity. In other terms, regularization prevents localization of the solutions at the material level, and thus maintains mesh-objectivity of the softening branch. The main ingredient of visco-plastic regularization is the relaxation time, τ that retains positive eigenvalues of the acoustic tensor, $\boldsymbol{Q}_{vp}$ as indicated in Figures 9 (c and d), 10(b), and 11(c). In other words, inclusion of viscosity prevents the material properties from localizing by delaying discontinuous bifurcation of the algorithmic tangent operator. The loss of ellipticity is induced when the linearized algebraic form turns zero, i.e. $\det(\boldsymbol{Q}_{vp}) = 0$. Thus stabilization of the localization tendencies is of great importance in the area of numerical solution schemes, since it prevents the formation of jump conditions due to spatial discontinuities.

The diagrams in Figures 9 (c and d), 10(b) and 11(c) illustrate the variation of the normalized localization tensor $\det(\boldsymbol{Q}_{vp})/\det(\boldsymbol{Q}_e)$ *vs.* the angle θ in the Duvaut-Lions formulation of the concrete model. In the case of inviscid elasto-plastic materials, the underlying tangent stiffness exhibits localization in uniaxial tension and shear (T-C), but not in uniaxial compression. In contrast, the rate-dependent visco-plastic results in Figures 9 (c and d) and 10(b) show regularized solutions ($\det(\boldsymbol{Q}_{vp}) > 0$) suppressing localization in tension and shear (T-C), where T-C denotes equibiaxial tension-compression. The figures demonstrate that the parameters τ and

Δt, which control the amount of inelastic degradation, result in large differences of localization properties along the three different load paths. In particular, Figures 9 (c and d) illustrate the sensitivities of the localization properties to the parameters, τ and Δt, respectively. Figure 9(c) exhibits that larger values of τ yield more elastic behavior, and vice versa. Figure 9(d) shows that smaller values of Δt show the same trend. Note, localization analyses in this study were performed at the point of elasto-plastic localization except for the results shown in Figures 9 (e and f).

Besides the localization properties at the material level, there is an additional issue to explore in the area of spatial discretization using finite elements. Due to spatial discretization of the continuum differential equations, mesh objective solutions are very difficult to obtain unless a characteristic length scale is introduced. Several regularization techniques such as fracture energy method (Willam et al., 1986), strong discontinuity method (Simo et al, 1993; Kang and Willam, 1996) introduce mesh objective solutions in terms of nominal stress *vs.* displacement response. In other words, regularization maintains the same fracture energy dissipation of the postpeak response in spite of discretization of specimen. In physical tests, the fracture energy dissipation remains the same when the crack surfaces are identical. The response behaviors under uniaxial tension depicted in Figure 12(a) in the form of nominal stress σ_N *versus* nominal strain ϵ_N, and in Figure 12(b) in the form of nominal stress σ_N *versus* axial displacement Δ_Z clearly illustrate the loss of mesh objectivity after localization in elasto-plastic solutions. However, the response behaviors of the visco-plastic material formulation in Figures 13 (a and b) show a systematic delay of localization. Thereby several meshes depicted in Figures 14(a) and 14 (b thru. d) in the form of deformed meshes were tested for the same purpose, and the results depicted in Figure 14(a) illustrate improved regularization when a finer mesh is used. In other words, localization during softening is delayed further, when the specimen is discretized with a finer mesh. To trigger localization, an imperfection of 0.5 % reduction of the axial strength was introduced in one of the elements. An interesting aspect is that the four element mesh in Figures 14 (a and b) delays localization more than the serial mesh in Figures 13 (b and d). Therefore, it may be expected that a finer mesh than the one in Figure 14(d) may prevent loss of ellipticity even longer.

5 Conclusions

Experimental test results of G-mix concrete in uniaxial compression and indirect tension agree fairly well with other test results and numerical simulations (Duvaut-Lions Visco-plasticity), although there were limitations on the range of high loading rates. Obviously this study needs further extension of more tests with the appropriate number of specimens and high rate dynamic impact testing. On the numerical side, different visco-plastic formulations such as the Perzyna-model or the 'fully consistent' overstress formulations are needed for further verifica-

tion of rate performance of concrete materials.

Besides the rate dependent behavior of concrete, the visco-plastic extension regularizes the onset of localization in the non-associated strain softening concrete model and thus delays the loss of ellipticity of rate-independent inviscid material descriptions.

Acknowledgments

The authors wish to thank Maj. Mike Chipley and AFOSR, for the partial support of this effort under grant F 49620-98-1-0159 to the University of Colorado, Boulder.

References

ASTM (1996) American Society for Testing and Materials, C496-96, ASTM Annual Book of Standards, ASTM, Philadelphia

Bachmann, H., (1993) *Die Massenträgheit in einem Pseudo-Stoffgesetz für Beton bei schneller Zugbeanspruchung*, Dissertation and Heft 19 der Schriftenreihe des Inst. f. Massivebau u. Baustofftechnologie, Universität Karlsruhe.

Bažant, Z.P., and Kazemi, M.T. (1990) "Determination of Fracture Energy, Process Zone Length and Brittleness Number form Size Effect, With Application to Rock and Concrete", *International Journal of Fracture*, 44, 111-131.

Bažant, Z.P., and Planas, J. (1998) *Fracture and Size Effect in Concrete and Other Quasibrittle Materials*, Boca Raton, CRC Press.

Bischoff, P.H., (1998) *Compressive Response of Concrete to Hard Impact*, Ph.D Dissertation, Imperial College of Science and Technology, London.

Carmona, S., Gettu, R., and Aguado, A. (1998) "Study of the post-peak behavior of concrete in the splitting-tension test", Proc. of FRAMCOS-3, H. Mihashi and K. Rokugo eds., AEDIFICATIO Publishers, Gifu, Japan, October 12-16, 1, 151-160.

Duvaut, G. and Lions, J.L. (1972) *Les Inéquations en Méchanique et en Physique*, Dunod, Paris, France.

Etse, G. and Willam, K. (1999) "Failure Analysis of Elasto-Viscoplastic Material Models," ASCE-JEM, 125, 60-69.

Kang, H.D., (1997) *Triaxial Constitutive Model for Plain and Reinforced Concrete Behavior*, Ph.D. Dissertation, University of Colorado Boulder.

Kang, H.D. and Willam, K.J., (1999) "Localization Characteristics of A Triaxial Concrete Model", in press, ASCE *Journal of Engineering Mechanics*, August, 1999.

Malvar, L.J., and Ross, C.A. (1998) "Review of Strain Rate Effects for Concrete in Tension", ACI *Materials Journal*, 95, 735-739.

Perzyna, P. (1966) "Fundamental Problems in Viscoplasticity." *Advances in Applied Mechanics*, Academic Press, New York, N.Y., 9, 244-368.

RILEM Technical Recommendations of the Testing and Use of Construction Materials, International Union of Testing and Research Laboratories for Materials and Structures, E&FN Spon, New York, 1994.

Timoshenko, S.P. and Goodier, J.N. (1970) *Theory of Elasticity*, 3^{rd} ed., McGraw-Hill, New York.

Wang, M.W., Sluys, L.J., and de Borst, R. (1997) "Viscoplasticity for Instabilities due to Strain Softening and Strain-Rate Softening." *I. J. Num. Meth. Eng.*, 40, 3839-3864.

Willam, K., Hurlbut, B., and Sture, S. (1986) "Experimental and Constitutive Aspects of Concrete Failure" *Proc. Japan-US Symp. on Finite Element Analysis of Reinforced Concrete Structures*, C. Meyer and H. Okamura (eds.), ASCE, New York, 226-254.

Specimen No.	Period [*sec*]	Strain Rate	Strength [*ksi*]	Ratio	Max Load [*kips*]
GCR 1	10	0.00125	4.3	1.1	121.24
GCR 2	6	0.00208	5.19	1.266	146.74
GCR 3	15000	8.33E-07	4.1	1.0	115.92
GCR 4	10	0.00125	4.67	1.139	132.04

Table 1: Compression Test of 6×12 cylinder. (GCR : G-Mix Compression test of Cylinder.)

Specimen No.	Period [*sec*]	Strain Rate	Strength [*ksi*]	Ratio	Max Load [*kips*]
GCP 1	5	0.02	6.85	1.096	109.6
GCP 2	10	0.01	7.20	1.152	115.2
GCP 3	10	0.01	6.97	1.115	111.5
GCP 4*	100	0.001	7.98	1.277	127.7
GCP 5	100	0.001	6.94	1.110	111.0
GCP 6*	720	0.000139	7.53	1.205	120.5
GCP 7	1000	0.0001	6.66	1.066	106.6
GCP 8	10000	0.00001	5.90	0.944	94.4
GCP 9*	10000	0.00001	5.11	0.818	81.8
GCP 10	100000	0.000001	6.32	1.011	101.1
GCP 11	100000	0.000001	6.25	1.0	100.0
GCP 12*	720	0.000139	5.70	0.912	91.2

Table 2: Compression Test of $4 \times 4 \times 8$ prism. (GCP : G-Mix Compression test of Prism, * tests are not done in the same environments as others.)

Specimen No.	Period [*sec*]	Strain Rate	Strength [*ksi*]	Ratio	Max Load [*kips*]
GTR 1	5	0.005	0.6	1.23	67.86
GTR 2	3	0.00833	0.59	1.21	66.68
GTR 3	7500	0.0000033	0.511	1.046	57.68
GTR 4	10000	0.0000025	0.488	1.0	55.17

Table 3: Tension Test of 6×12 cylinder. (GTR : G-Mix Tension test of Cylinder.)

Specimen No.	Period [*sec*]	Strain Rate	Strength [*ksi*]	Ratio	Max Load [*kips*]
GTC 1	5	0.02	0.371	1.094	9.324
GTC 2	10	0.01	0.357	1.053	8.972
GTC 3	100	0.001	0.313	0.923	7.867
GTC 4	100	0.001	0.378	1.115	9.5
GTC 5	100	0.001	0.357	1.053	8.972
GTC 6	1000	0.0001	0.347	1.023	8.721
GTC 7	10000	0.00001	0.357	1.053	8.972
GTC 8	50000	0.000002	0.339	1.0	8.52
GTC 9	100000	0.000001	0.409	1.206	10.279

Table 4: Tension Test of $4 \times 4 \times 4$ cube. (GTC : G-Mix Tension test of Cube.)

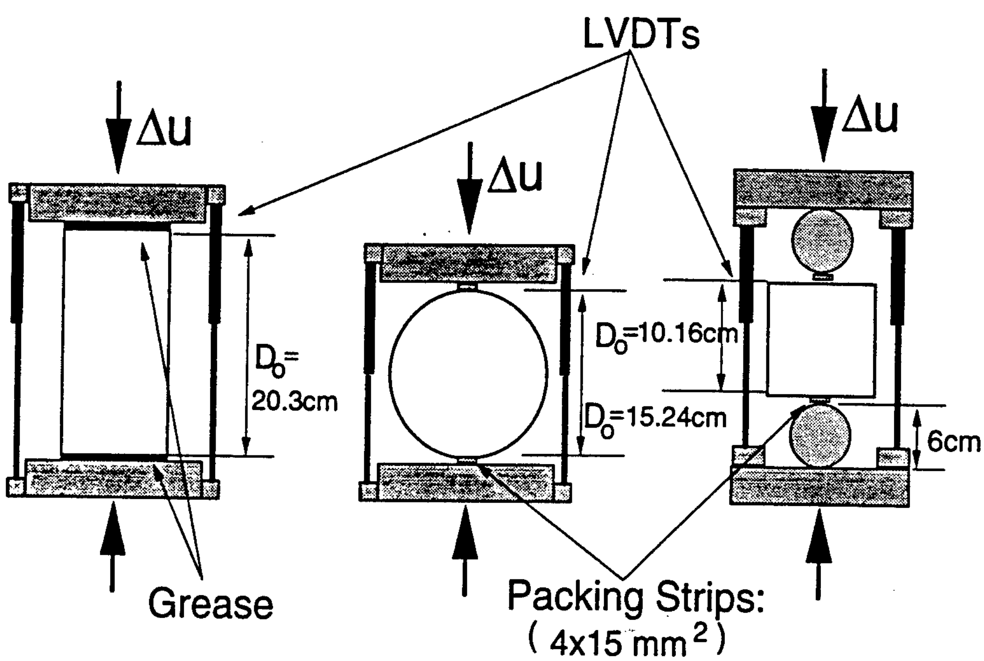

Figure 1: Test setup and geometry

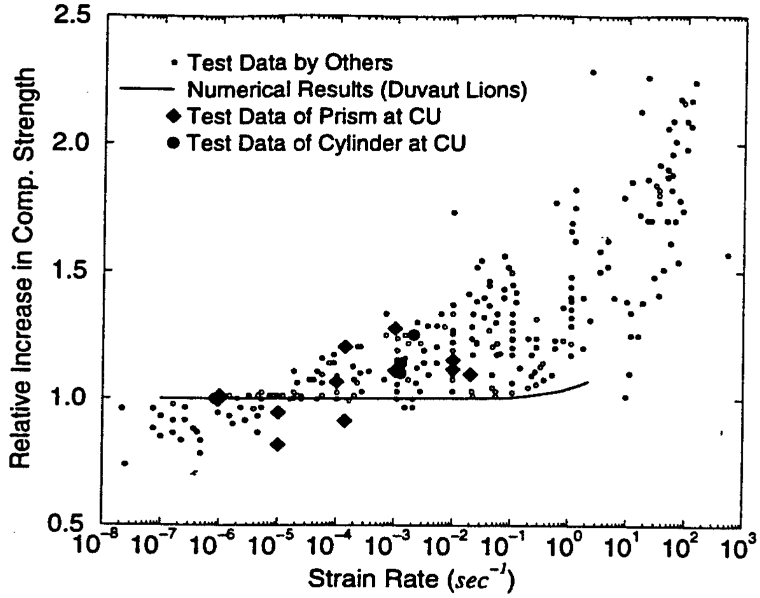

Figure 2: Dynamic strength enhancement under uniaxial compression in concrete, comparison with other data.

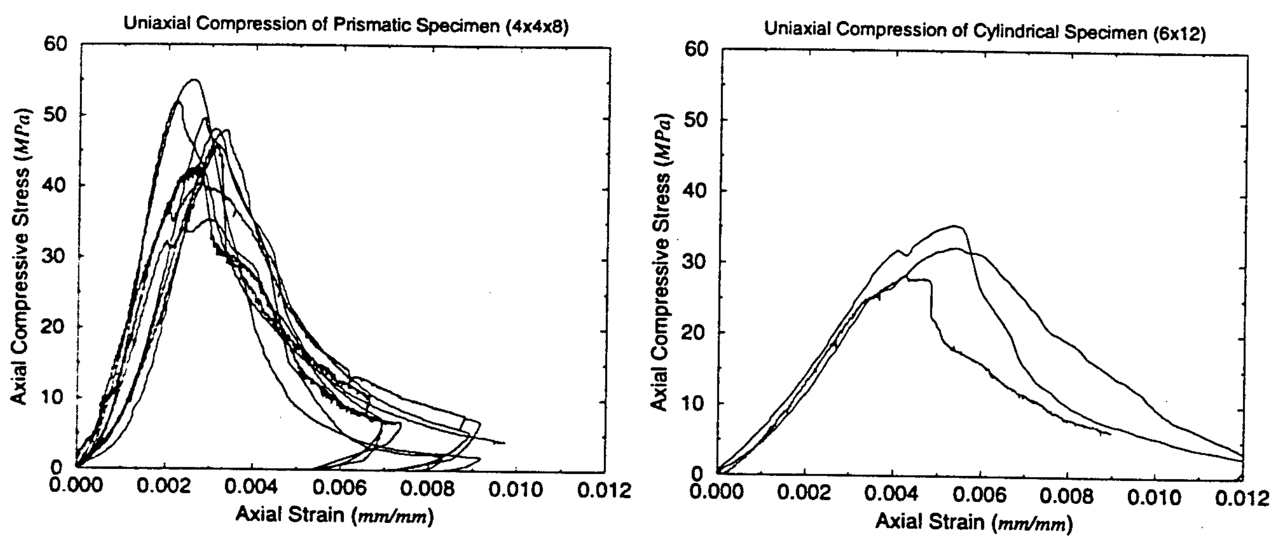

Figure 3: Nominal stress *vs.* strain responses of (a) prismatic and (b) cylindrical specimens under uniaxial compression.

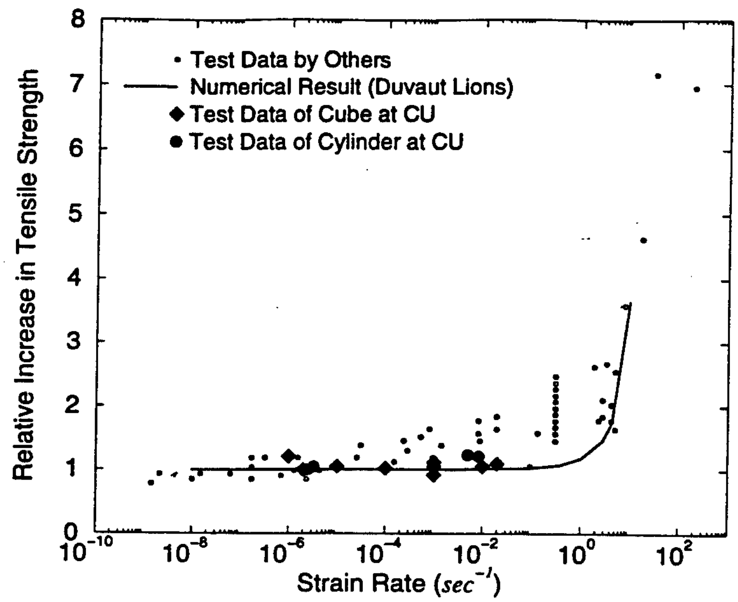

Figure 4: Dynamic strength enhancement under splitting tension in concrete, comparison with other data.

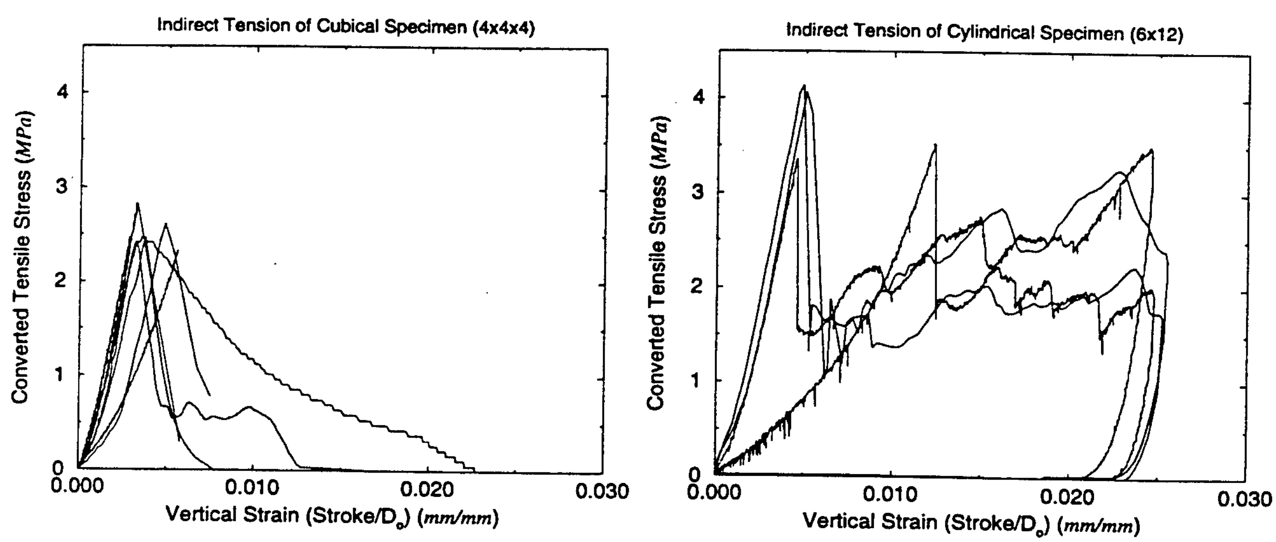

Figure 5: Nominal stress *vs.* axial strain responses of (a) cubical and (b) cylindrical specimens under splitting tension.

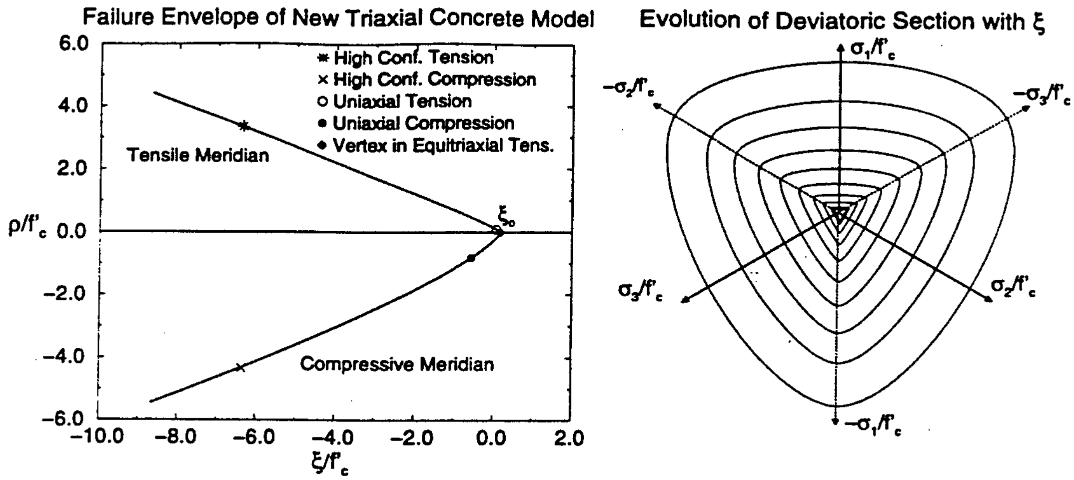

Figure 6: (a) Tensile and compressive meridians, (b) deviatoric tracings of triaxial concrete model.

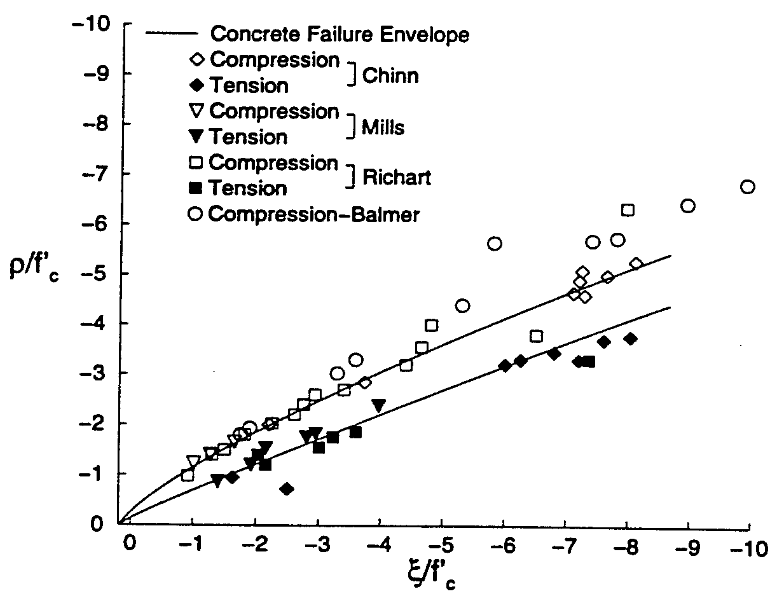

Figure 7: Performance of the concrete model in the triaxial stress space.

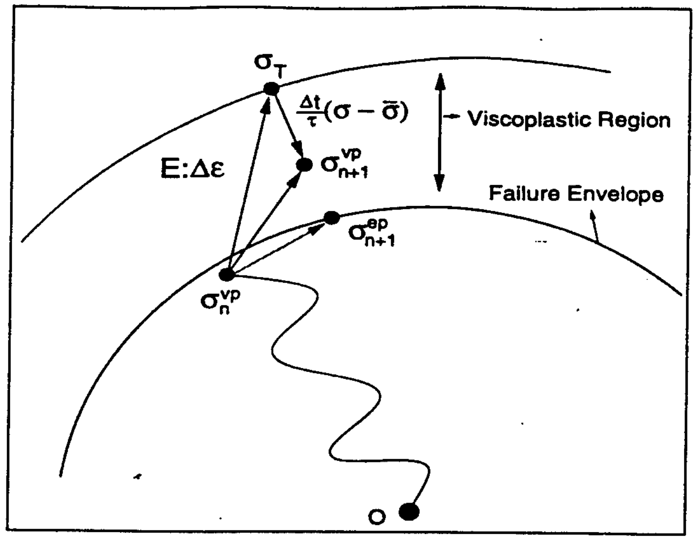

Figure 8: Visco-plastic process at the constitutive level.

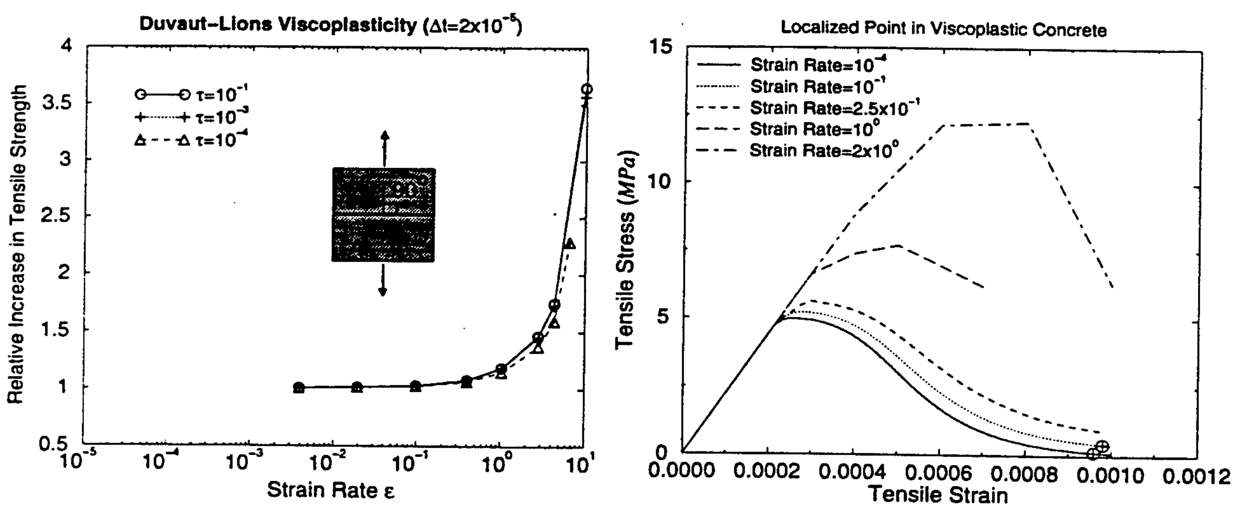

Figure 9: (a) Dynamic strength enhancement, and (b) axial stress *vs.* strain response at different loading rates in uniaxial tension.

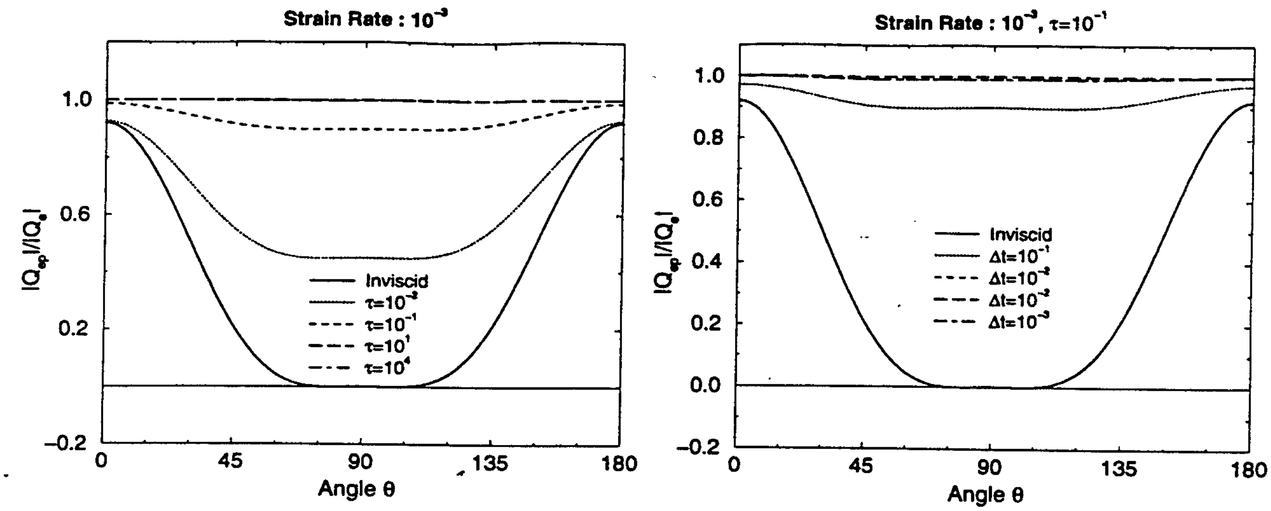

Figure 9: Localization Analysis for Duvaut-Lions visco-plasticity: sensitivities for regularized behaviors with (c) varying relaxation time, τ, and (d) varying Δt.

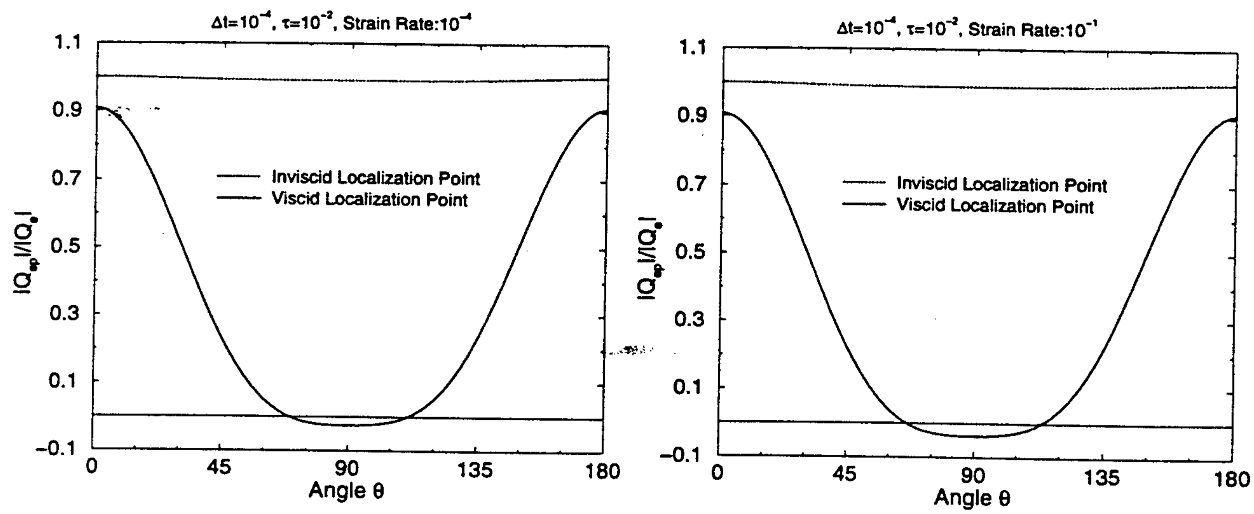

Figure 9: Localization indicators showing negative eigenvalues at strain rate, (e) 10^{-4}, and (f) 10^{-1}.

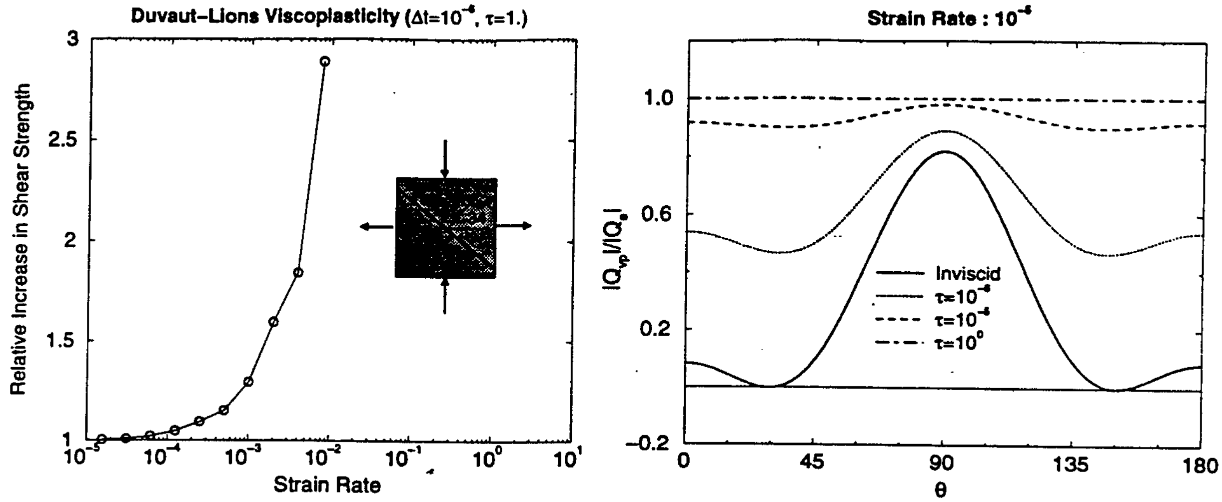

Figure 10: (a) Dynamic strength enhancement at different loading rates in equibiaxial tension-compression, and (b) localization analysis for Duvaut-Lions visco-plasticity: sensitivity for regularized behaviors with varying relaxation time, τ .

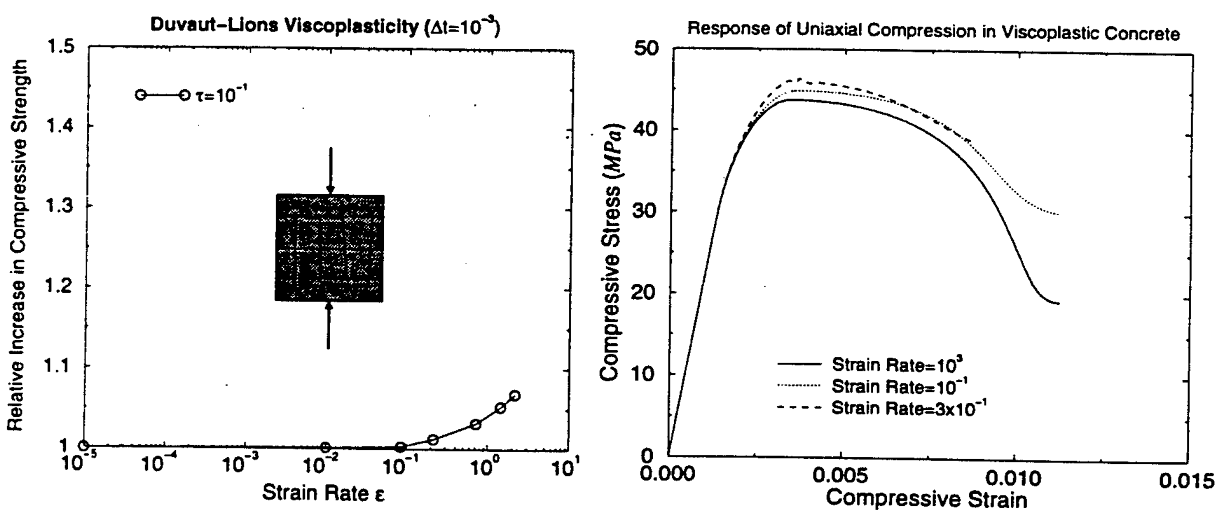

Figure 11: (a) Dynamic strength enhancement, and (b) axial stress *vs.* strain response at different loading rates in uniaxial compression.

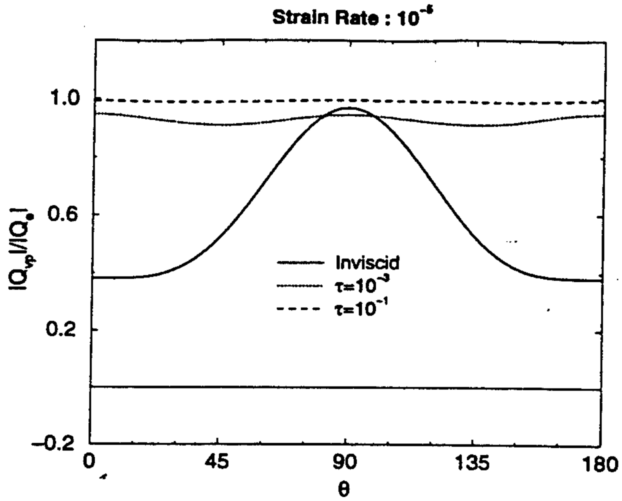

Figure 11: (c) Localization analysis for Duvaut-Lions visco-plasticity: sensitivity with varying relaxation time, τ .

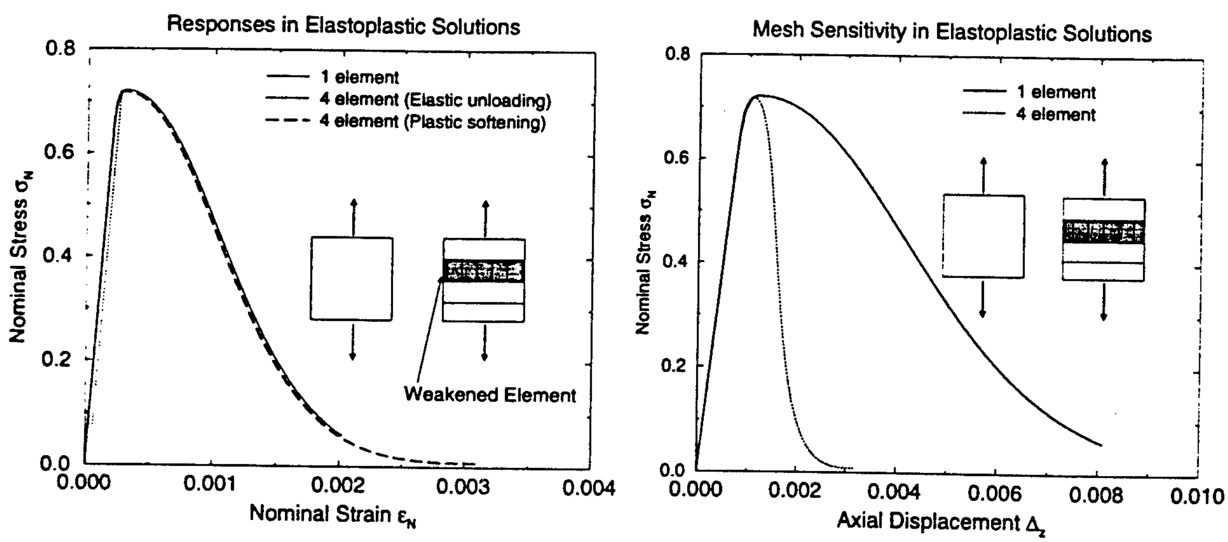

Figure 12: (a) Response and (b) mesh sensitivity of one *vs.* four (serial) element mesh in elasto-plastic concrete formulation under uniaxial tension.

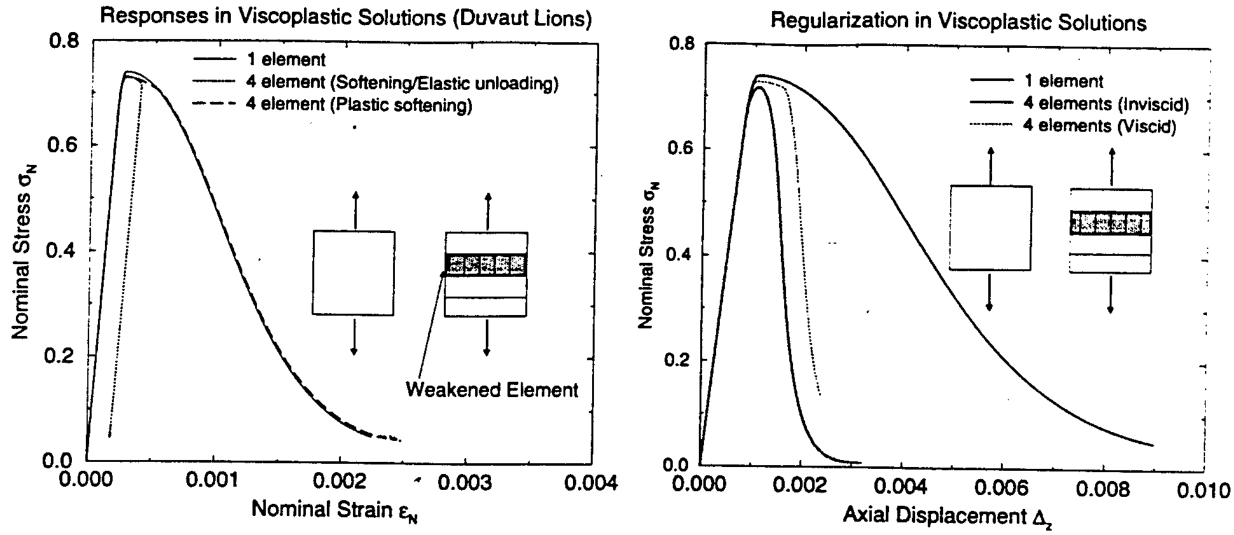

Figure 13: (a) Response and (b) regularized mesh sensitivity of one *vs.* four (serial) element mesh in visco-plastic concrete formulation under uniaxial tension.

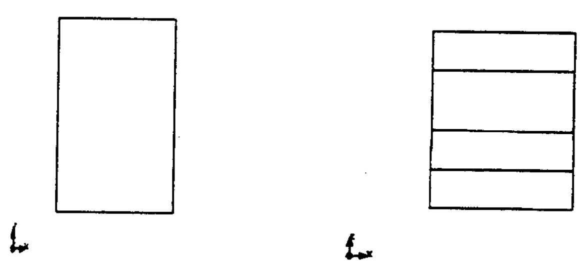

Figure 13: Deformed mesh of (c) one and (d) four (serial) element meshes.

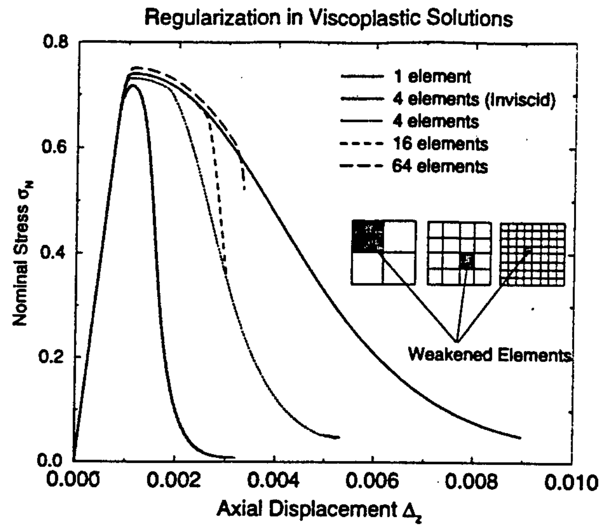

Figure 14: (a) Improved regularization of 4, 16 and 64 element meshes in visco-plastic concrete formulation under uniaxial tension.

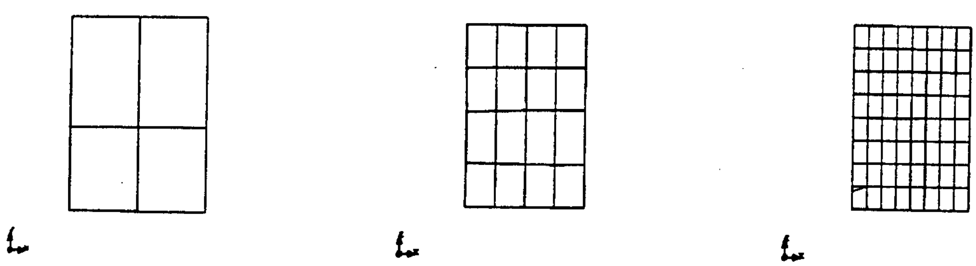

Figure 14: Deformed mesh of (b) 4, (c) 16 and (d) 64 element meshes.